# Self-propelled particles with selective attraction-repulsion interaction - From microscopic dynamics to hydrodynamics

**R Großmann[1], L Schimansky-Geier[1] and P Romanczuk[2]**

[1] Department of Physics, Humboldt-Universität zu Berlin, Newtonstr. 15, 12489 Berlin, Germany
[2] Max Planck Institute for the Physics of Complex Systems, Nöthnitzerstr. 38, 01187 Dresden, Germany

E-mail: `prom@pks.mpg.de`

**Abstract.** In this work we derive and analyze coarse-grained descriptions of self-propelled particles with selective attraction-repulsion interaction, where individuals may respond differently to their neighbours depending on their relative state of motion (approach versus movement away). Based on the formulation of a nonlinear Fokker-Planck equation, we derive a kinetic description of the system dynamics in terms of equations for the Fourier modes of a one-particle density function. This approach allows effective numerical investigation of the stability of possible solutions of the system. The detailed analysis of the interaction integrals entering the equations demonstrates that divergences at small wavelengths can appear at arbitrary expansion orders.

Further on, we also derive a hydrodynamic theory by performing a closure at the level of the second Fourier mode of the one-particle density function. We show that the general form of equations is in agreement with the theory formulated by Toner and Tu.

Finally, we compare our analytical predictions on the stability of the disordered homogeneous solution with results of individual-based simulations. They show good agreement for sufficiently large densities and non-negligible short-ranged repulsion. Disagreements of numerical results and the hydrodynamic theory for weak short-ranged repulsion reveal the existence of a previously unknown phase of the model consisting of dense, nematically aligned filaments, which cannot be accounted for by the present Toner and Tu type theory of polar active matter.

## 1. Introduction

In recent decades, there has been an increased research focus on far-from-equilibrium systems in biology and physics which is referred to as "active matter". The relevant length scales of such systems span several orders of magnitude. They range from the (sub-)micrometer scale governing the dynamics of individual active units in motility assays in-vitro [1] and the actin cortex in-vivo [2], via the mesoscopic length scales of interest in collective dynamics of large bacterial ensembles [3, 4] and artificial self-propelled particles [5], up to the macroscopic scales of driven granular matter [6, 7] or flocks of birds [8], schools of fish [9], and swarms of insects [10, 11], where the spatial dimensions can be in the order of kilometers.

Despite the apparent variety, all these systems share the fundamental property of local uptake and/or conversion of internal energy into kinetic energy of motion by its individual units. This – together with additional interactions between those units – distinguishes this systems from related equilibrium systems and yields fascinating examples of self-organization and collective dynamics.

The question of universal properties of such active matter systems from the statistical physics point of view is a vibrant research field. To a large extent, it was initiated by the numerical study of a minimal, individual-based model of active matter published by Vicsek *et al* in 1995 [12]. Shortly after this publication, Toner and Tu made a seminal contribution by formulating the hydrodynamic equations of polar active matter at largest relevant length and time scales purely based on symmetry arguments [13, 14]. The analysis of this generic equations, as well as their counterparts for nematic order, improved our understanding of the fundamental properties of active matter, such as the existence of long range order or giant number fluctuations [15, 16].

However, the direct derivation of a hydrodynamic theory of the Toner and Tu type from microscopic models of active matter was a long standing problem. Only recently, such a link between microscopic parameters determining the dynamics of individual active units and parameters governing the macroscopic flow of active matter was established by formulating kinetic equations for minimal models of self-propelled particles with velocity-alignment [17–20] and self-propelled aligning rods [21]. Furthermore, coarse-grained descriptions for active particles with variable speeds and velocity-alignment were derived in [22–26].

In this paper, we will derive a kinetic and a hydrodynamic description for self-propelled agents interacting via a selective attraction and repulsion interaction. A corresponding model was recently introduced to describe the onset of collective motion in insect swarms and is directly motivated by response of individual agents to looming visual stimuli [27, 28]. The model shows different phases including large scale collective motion, a disordered clustering phase and a nematic phase despite the absence of an explicit velocity-alignment interaction.

First, we will introduce the microscopic, individual-based model in terms of stochastic differential equations. Then we will proceed with the discussion of a kinetic

description of the collective dynamics based on the nonlinear Fokker-Planck equation for the one-particle density function, which allows efficient numerical analysis of the stability of solutions of the Fokker-Planck equation (especially the spatially homogeneous, disordered state) in Fourier space. Further on, we will derive a hydrodynamic theory for self-propelled particles with selective attraction-repulsion interaction, which yields hydrodynamic equations in agreement with the theory by Toner and Tu. A direct comparison of the kinetic approach, which in principle can be considered up to arbitrary accuracy, to the hydrodynamic theory, which corresponds to a closure at the level of the second Fourier mode of the probability density function, reveals the range of validity of the hydrodynamic equations at large wavenumbers. Moreover, the analysis provides insights into the origin of unphysical divergences at large wavenumbers related to the approximations used namely the usage of Taylor polynomials. Finally, we compare the results of the kinetic and hydrodynamic theory with direct numerical simulations of the individual-based model.

## 2. Microscopic Model

We consider $N$ self-propelled particles of mass $m = 1$ in two spatial dimensions, so-called agents. Each individual moves at a constant speed $s_0$, thus the velocity vector of each agent is determined by its polar orientation angle $\varphi_i$. The equations of motion for the positions $\boldsymbol{r}_i$ and the polar orientation angles $\varphi_i$ read:

$$\frac{\mathrm{d}\boldsymbol{r}_i}{\mathrm{d}t} = s_0 \boldsymbol{e}_{i,h}(t) = s_0 \begin{pmatrix} \cos\varphi_i(t) \\ \sin\varphi_i(t) \end{pmatrix}, \tag{2.1a}$$

$$\frac{\mathrm{d}\varphi_i}{\mathrm{d}t} = \frac{1}{s_0}\left(F_{i,\varphi} + \sqrt{2D_\varphi}\,\xi_i(t)\right). \tag{2.1b}$$

Here, $F_{i,\varphi} = \boldsymbol{F}_i\,\boldsymbol{e}_{i,\varphi}$ is the projection of an effective social force vector $\boldsymbol{F}_i$ on the angular degree of freedom $\varphi_i$, which induces a turning behaviour of the focal individual due to interaction with others. $\boldsymbol{e}_{i,\varphi} = (-\sin\varphi_i, \cos\varphi_i)^T$ is the angular unit vector perpendicular to $\boldsymbol{e}_{i,h}$.

The second term within the brackets in (2.1b) stands for random angular noise with intensity $D_\varphi$. $\xi_i(t)$ are independent, Gaussian random processes with vanishing mean and temporal $\delta$-correlations, i.e. $\langle\xi_i(t)\xi_j(t+\tau)\rangle = \delta_{ij}\,\delta(\tau)$ (Gaussian white noise).

The total social force is given by a sum of three components:

$$\boldsymbol{F}_i = \boldsymbol{f}_{i,r} + \boldsymbol{f}_{i,m} + \boldsymbol{f}_{i,a}. \tag{2.2}$$

The first term represents a short-ranged repulsion allowing for finite sized agents. It reads

$$\boldsymbol{f}_{i,r} = -\sum_{j=1}^{N} \mu_r(r_{ji})\hat{\boldsymbol{r}}_{ji}\theta(l_c - r_{ji}) \tag{2.3}$$

with $\mu_r(r_{ji}) \geq 0$ being a repulsive turning rate, which in general depends on distance $r_{ji} = |\boldsymbol{r}_{ji}| = |\boldsymbol{r}_j - \boldsymbol{r}_i|$ between two particles. We assume that this repulsive interaction

is strictly short-ranged, i.e. it vanishes above a finite repulsive radius $l_c$, as indicated by the Heaviside (unit-step) function $\theta(x)$.

The other two forces read:

$$\boldsymbol{f}_{i,m} = \sum_{j=1}^{N} \mu_m(r_{ji}) \, |\tilde{v}_{ji}| \, \hat{\boldsymbol{r}}_{ji} \theta(l_s - r_{ji}) \theta(r_{ji} - l_c) \theta(\tilde{v}_{ji}), \tag{2.4a}$$

$$\boldsymbol{f}_{i,a} = \sum_{j=1}^{N} \mu_a(r_{ji}) \, |\tilde{v}_{ji}| \, \hat{\boldsymbol{r}}_{ji} \theta(l_s - r_{ji}) \theta(r_{ji} - l_c) \theta(-\tilde{v}_{ji}). \tag{2.4b}$$

These forces can be considered as a sum over pairwise interactions, which act always along the unit vector $\hat{\boldsymbol{r}}_{ji} = (\boldsymbol{r}_j - \boldsymbol{r}_i)/r_{ji}$ pointing towards the center of mass of the neighbouring particle $j$. The corresponding response strengths $\mu_{a,m}(r_{ji})$ are distance dependent and may in general be both positive (attraction) and negative (repulsion). Furthermore, the overall response to other individuals is assumed to vanish above a finite sensory range $l_s$: $\mu_{a,m}(r_{ji} > l_s) = 0$, whereby $l_s \geq l_c$.

The decisive factor in the distinction of the two forces is the sign of the relative velocity $\tilde{v}_{ji}$ defined by the temporal derivative of the distance $r_{ji}$ between particles $i$ and $j$, and equals the projection of the velocity difference $\mathbf{v}_{ji} = \mathbf{v}_j - \mathbf{v}_i$ of neighbour $j$ and the focal individual $i$ on the relative position unit vector $\hat{\boldsymbol{r}}_{ji}$. $\boldsymbol{f}_{i,a}$ is the response to approaching individuals characterized by a negative relative velocity $\tilde{v}_{ji} < 0$, whereas $\boldsymbol{f}_{i,m}$ is the corresponding response to moving away (or receding) individuals characterized by positive relative velocity $\tilde{v}_{ji} > 0$. Both force terms are proportional to the absolute value of the relative velocity, leading to stronger responses to faster approaching or receding individuals. Using the definition $\tilde{v}_{ji} = \dot{r}_{ji}$, one obtains the relative velocity

$$\tilde{v}_{ji} = \tilde{v}_{ji}(\varphi_i, \varphi_j, \alpha_{ji}) = 2s_0 \sin\left(\frac{\varphi_j + \varphi_i}{2} - \alpha_{ji}\right) \sin\left(\frac{\varphi_i - \varphi_j}{2}\right) \tag{2.5}$$

as a function of the velocity angles $\varphi_i$, $\varphi_j$ and the angle $\alpha_{ji}$ of the distance vector $\boldsymbol{r}_{ji}$, with $\boldsymbol{r}_{ji} = r_{ji}(\cos\alpha_{ji}, \sin\alpha_{ji})$. From (2.5), one finds the two different spatial regions of approaching and receding particles, respectively, where the relative velocity has a different sign for fixed $\varphi_i$ and $\varphi_j$ in the interval $\varphi_i \leq \varphi_j < \varphi_i + 2\pi$:

$$\begin{array}{llll} v_{ji} > 0 & \text{for} & \frac{\varphi_j + \varphi_i}{2} < \alpha_{ji} < \frac{\varphi_j + \varphi_i}{2} + \pi & \text{moving away,} \\ v_{ji} < 0 & \text{for} & \frac{\varphi_j + \varphi_i}{2} + \pi < \alpha_{ji} < \frac{\varphi_j + \varphi_i}{2} + 2\pi & \text{approaching.} \end{array} \tag{2.6}$$

Hence, a particle located in the half-sphere in clockwise direction from the mean angle $(\varphi_j + \varphi_i)/2$ approaches the focal particle $i$, whereas particles located in the other half-sphere anticlockwise from the mean angle are moving away (see figure 1). Please note that for $\varphi_j = \varphi_i$ the social force vanishes as $\tilde{v}_{ji} = 0$ according to (2.5).

Four different regions in the $(\mu_m, \mu_a)$-parameter space are distinguished [28]:

- Pure Repulsion: $\mu_m < 0$, $\mu_a < 0$;

- Escape/Pursuit: $\mu_m > 0$, $\mu_a < 0$, i.e. attraction to particles moving away, repulsion from particles coming closer;
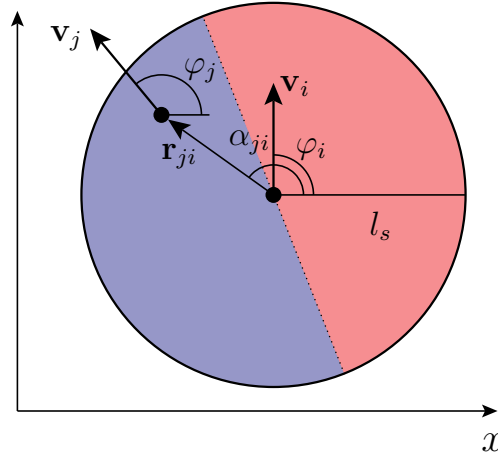
**Figure 1.** Visualization of the spatial regions for approaching and receding self-propelled particles for a binary interaction of the $i$th particle with velocity vector $\mathbf{v}_i$ (heading angle $\varphi_i$), and a neighbouring particle $j$ with velocity $\mathbf{v}_j$ (heading angle $\varphi_j$) within its sensory range $l_s$. The center of the circle corresponds to the position of the focal particle $i$. The dotted line, determined by the mean angle $(\varphi_i + \varphi_j)/2$, represents the border between the two distinct spatial regions (half-discs) corresponding to approaching and moving away of individual $j$. If the $j$th particle is located above the dotted line in the red region, the two particles are coming closer (approaching). Otherwise, if the neighbouring particle is located in the blue region, the two particles move away from each other (as shown in this example).

- Head on Head: $\mu_m < 0$, $\mu_a > 0$, i.e. attraction to particles coming closer, repulsion from particles moving away;

- Pure Attraction: $\mu_m > 0$, $\mu_a > 0$.

Some typical spatial snapshots obtained from individual-based simulations of (2.1) are shown in figure 2.

The above microscopic model corresponds to the ones studied in [27, 28], if the distance dependent interaction strengths $\mu_r(r_{ji})$ and $\mu_{a,m}(r_{ji})$ are assumed to be constant and the forces are rescaled by the number of particles within the interaction area of the focal particle.

## 3. Kinetic Description

In this section, we derive a kinetic description for the above individual-based model (2.1). For this purpose, we introduce the $N$-particle probability density function (PDF)

$$P_N(\boldsymbol{r}_1, \varphi_1; \boldsymbol{r}_2, \varphi_2; \ldots; \boldsymbol{r}_N, \varphi_N; t)\,, \tag{3.1}$$

which determines the probability to find particle $i$ at position $\boldsymbol{r}_i$ moving into the direction $\varphi_i$ $(i = 1, 2, \ldots, N)$ at time $t$. It is normalized with respect to integration over all
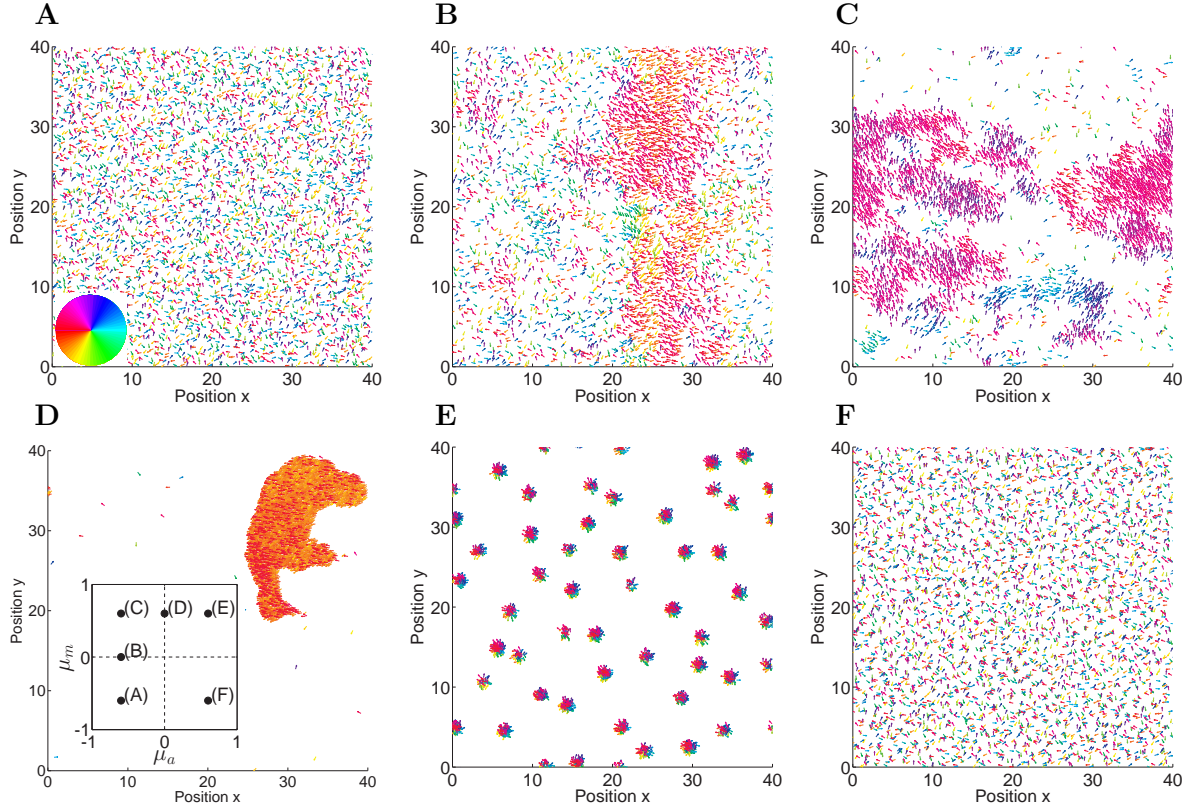
**Figure 2.** Spatial snapshots of the microscopic model for different interaction strengths after the system relaxes towards a steady-state: (A) disordered, homogeneous state for $\mu_a = \mu_m = -0.6$ (pure repulsion), (B) diffuse collectively moving bands for $\mu_a = -0.6$, $\mu_m = 0$ (only escape), (C) collectively moving bands for $\mu_a = -0.6$, $\mu_m = 0.6$ (escape and pursuit), (D) dense, collectively moving cluster for $\mu_m = 0.6$, $\mu_a = 0$ (only pursuit), (E) cluster state for $\mu_m = \mu_a = 0.6$ (pure attraction), (F) disordered, homogeneous state for $\mu_m = -0.6$, $\mu_a = 0.6$ (head on head). The velocity vectors of individual particles are coloured corresponding to their polar direction of motion according to the inset of (A). The inset in (D) indicates the positions of the snapshots in the $(\mu_a, \mu_m)$-parameter plane. Other parameters: $N = 4000$, $L = 40$, $D_\varphi = 0.02$, $l_s = 1$, $l_c = 0.2$, $\mu_r = 5$, $s_0 = 0.25$.

positions and angles:

$$\prod_{j=1}^{N} \left( \int \mathrm{d}^2 r_j \int_0^{2\pi} \mathrm{d}\varphi_j \right) P_N(\boldsymbol{r}_1, \varphi_1; \boldsymbol{r}_2, \varphi_2; \ldots; \boldsymbol{r}_N, \varphi_N; t) = 1 \,. \tag{3.2}$$

In agreement with (2.1), we can write down the Fokker-Planck equation (FPE) for the dynamics of the PDF as follows.

$$\frac{\partial P_N}{\partial t} = -s_0 \sum_{i=1}^{N} \nabla_{\boldsymbol{r}_i} \left( \boldsymbol{e}_{i,h} P_N \right) - \sum_{i=1}^{N} \frac{\partial}{\partial \varphi_i} \left( \frac{F_{i,\varphi} P_N}{s_0} \right) + \frac{D_\varphi}{s_0^2} \sum_{i=1}^{N} \frac{\partial^2 P_N}{\partial \varphi_i^2} \tag{3.3}$$

From the linear FPE above one can derive an evolution equation for the marginal PDF

$$P(\boldsymbol{r}_i, \varphi_i, t) = \prod_{j \neq i}^{N} \left( \int \mathrm{d}^2 r_j \int_0^{2\pi} \mathrm{d}\varphi_j \right) P_N(\boldsymbol{r}_1, \varphi_1; \boldsymbol{r}_2, \varphi_2; \dots; \boldsymbol{r}_N, \varphi_N; t) \quad (3.4)$$

by integrating (3.3) over the degrees of freedom of particles $j \neq i$. In what follows, we assume that correlations between particles can be neglected. Therefore, the $N$-particle PDF shall factorize, i.e.

$$P_N(\boldsymbol{r}_1, \varphi_1; \boldsymbol{r}_2, \varphi_2; \dots; \boldsymbol{r}_N, \varphi_N; t) = \prod_{i=1}^{N} P(\boldsymbol{r}_i, \varphi_i, t). \quad (3.5)$$

By this means, one obtains an effective one-particle description

$$\frac{\partial P(\boldsymbol{r}_i, \varphi_i, t)}{\partial t} = -s_0 \nabla_{\boldsymbol{r}_i} (\boldsymbol{e}_{i,h} P) - \frac{N-1}{s_0} \frac{\partial}{\partial \varphi_i} (F_\varphi P) + \frac{D_\varphi}{s_0^2} \frac{\partial^2 P}{\partial \varphi_i^2}, \quad (3.6)$$

where the force $F_\varphi$ is given by the following integral over $P(\boldsymbol{r}_i, \varphi_i, t)$:

$$F_\varphi(\boldsymbol{r}_i, \varphi_i, t) = 2s_0 \int_{\varphi_i}^{\varphi_i+2\pi} \mathrm{d}\varphi_j \, \sin\left( \frac{\varphi_i - \varphi_j}{2} \right) \int_{l_c}^{l_s} \mathrm{d}r_{ji} \, r_{ji}$$

$$\left[ \mu_m(r_{ji}) \int_{\frac{\varphi_i+\varphi_j}{2}}^{\frac{\varphi_i+\varphi_j}{2}+\pi} \mathrm{d}\alpha_{ji} \, \sin(\alpha_{ji} - \varphi_i) \sin\left( \frac{\varphi_i + \varphi_j}{2} - \alpha_{ji} \right) P(\boldsymbol{r}_i + \boldsymbol{r}_{ji}, \varphi_j, t) \right.$$

$$\left. -\mu_a(r_{ji}) \int_{\frac{\varphi_i+\varphi_j}{2}+\pi}^{\frac{\varphi_i+\varphi_j}{2}+2\pi} \mathrm{d}\alpha_{ji} \, \sin(\alpha_{ji} - \varphi_i) \sin\left( \frac{\varphi_i + \varphi_j}{2} - \alpha_{ji} \right) P(\boldsymbol{r}_i + \boldsymbol{r}_{ji}, \varphi_j, t) \right]$$

$$- \int_{\varphi_i}^{\varphi_i+2\pi} \mathrm{d}\varphi_j \int_0^{l_c} \mathrm{d}r_{ji} \, r_{ji} \int_0^{2\pi} \mathrm{d}\alpha_{ji} \, \mu_r(r_{ji}) \sin(\alpha_{ji} - \varphi_i) P(\boldsymbol{r}_i + \boldsymbol{r}_{ji}, \varphi_j, t). \quad (3.7)$$

The factor $N - 1$ in (3.6) arises, because (3.3) was integrated over the positions and angles of $N - 1$ identical particles. In other words, the focal particle can interact with $N - 1$ neighbours. For the same reason, the particle index $i$ is omitted henceforward.

Please note, that a nonlinear FPE (3.6) for the dynamics of $P(\boldsymbol{r}, \varphi, t)$ was derived from a linear FPE (3.3) governing the dynamics of $P_N$. Equation (3.6) is nonlinear since the interaction force $F_\varphi$ depends on the probability density $P(\boldsymbol{r}, \varphi, t)$. In this sense, assumption (3.5) is a mean-field approximation: a single particle is affected by a force due to its own PDF (3.7).

By introducing the one-particle density function $p(\boldsymbol{r}, \varphi, t) = NP(\boldsymbol{r}, \varphi, t)$ we can eliminate the factor $(N - 1) \approx N$ from (3.6). Accordingly, $p(\boldsymbol{r}, \varphi, t)$ is interpreted as particle density obeying the nonlinear Fokker-Planck equation

$$\frac{\partial p(\boldsymbol{r}, \varphi, t)}{\partial t} = -s_0 \nabla_{\boldsymbol{r}} (\boldsymbol{e}_h p) - \frac{\partial}{\partial \varphi} \frac{F_\varphi(\boldsymbol{r}, \varphi, t) \, p}{s_0} + \frac{D_\varphi}{s_0^2} \frac{\partial^2 p}{\partial \varphi^2}. \quad (3.8)$$

One solution to the equation is the uniform distribution (spatially homogeneous, disordered state), i.e.

$$p^{(0)} = \frac{\rho_0}{2\pi}, \quad (3.9)$$

where $\rho_0 = N/L^2$ is the homogeneous particle density and $L$ denotes the linear spatial dimension of the two-dimensional square-shaped system.

### 3.1. Stability Analysis in Fourier Space

In order to analyze the Fokker-Planck equation (3.8) analytically and especially to solve the integral (3.7), it is convenient to work in Fourier space with respect to the spatial coordinates $\boldsymbol{r}$ and the angular variable $\varphi$. The dynamics of the Fourier coefficients

$$\hat{g}_n(\boldsymbol{k}, t) = \int \mathrm{d}^2 r \int_0^{2\pi} \mathrm{d}\varphi \, p(\boldsymbol{r}, \varphi, t) e^{i\boldsymbol{k}\boldsymbol{r} + in\varphi} \tag{3.10}$$

reads

$$\frac{\partial \hat{g}_n(\boldsymbol{k}, t)}{\partial t} - \frac{ik_x s_0}{2} (\hat{g}_{n+1} + \hat{g}_{n-1}) - \frac{k_y s_0}{2} (\hat{g}_{n+1} - \hat{g}_{n-1}) = -n^2 \frac{D_\varphi}{s_0^2} \hat{g}_n$$

$$+ \frac{in}{(2\pi)^3 s_0} \sum_{j=-\infty}^{\infty} \int \mathrm{d}^2 q \, \hat{g}_j(\boldsymbol{q}, t) \hat{K}_{n-j}(\boldsymbol{k} - \boldsymbol{q}, t), \tag{3.11}$$

where the Fourier coefficients of the force (3.7) are defined as

$$\hat{K}_n(\boldsymbol{k}, t) = \int \mathrm{d}^2 r \int_0^{2\pi} \mathrm{d}\varphi \, F_\varphi(\boldsymbol{r}, \varphi, t) e^{i\boldsymbol{k}\boldsymbol{r} + in\varphi}. \tag{3.12}$$

Obviously, the Fokker-Planck equation turns into an infinite hierarchy of equations (3.11) in Fourier space.

In this section it is shown, how the stability of the uniform distribution (3.9) can be analyzed in Fourier space. Furthermore, some difficulties associated with the derivation of hydrodynamic equations, as done in section 4, are outlined. A similar approach was used by Chou *et al* in order to achieve a kinetic theory for self-propelled particles with metric-free interactions [29].

For the stability analysis, the Fourier coefficients $\hat{K}_n(\boldsymbol{k}, t)$ of the force (3.7) are required. Due to the fact, that the force $F_\varphi(\boldsymbol{r}, \varphi, t)$ depends on the integral over $p(\boldsymbol{r}, \varphi, t)$ (3.7), the Fourier coefficients $\hat{K}_n(\boldsymbol{k}, t)$ of the force can be written as a linear combination of the Fourier coefficients $\hat{g}_r(\boldsymbol{k}, t)$

$$\hat{K}_n(\boldsymbol{k}, t) = \sum_{r=-\infty}^{\infty} \tilde{K}_{n,r}(\boldsymbol{k}) \hat{g}_r(\boldsymbol{k}, t) \tag{3.13}$$

using an infinite dimensional matrix $\tilde{K}_{n,r}(\boldsymbol{k})$. More details on the calculation of the matrix elements are given in Appendix A. Consequently, the nonlinear Fokker-Planck equations reads

$$\frac{\partial \hat{g}_n(\boldsymbol{k}, t)}{\partial t} - \frac{ik_x s_0}{2} (\hat{g}_{n+1} + \hat{g}_{n-1}) - \frac{k_y s_0}{2} (\hat{g}_{n+1} - \hat{g}_{n-1}) = -n^2 \frac{D_\varphi}{s_0^2} \hat{g}_n$$

$$+ \frac{in}{(2\pi)^3 s_0} \sum_{j=-\infty}^{\infty} \sum_{r=-\infty}^{\infty} \int \mathrm{d}^2 q \, \hat{g}_j(\boldsymbol{q}, t) \hat{g}_r(\boldsymbol{k} - \boldsymbol{q}, t) \tilde{K}_{n-j,r}(\boldsymbol{k} - \boldsymbol{q}). \tag{3.14}$$

Let $\hat{g}_n^{(0)}(\boldsymbol{k}, t)$ be a solution of the equation above. The dynamics of a small perturbation $\delta\hat{g}_n(\boldsymbol{k}, t) = \hat{g}_n(\boldsymbol{k}, t) - \hat{g}_n^{(0)}(\boldsymbol{k}, t)$ is determined by the linearized equation

$$\frac{\partial \delta\hat{g}_n(\boldsymbol{k}, t)}{\partial t} - \frac{ik_x s_0}{2} (\delta\hat{g}_{n+1} + \delta\hat{g}_{n-1}) - \frac{k_y s_0}{2} (\delta\hat{g}_{n+1} - \delta\hat{g}_{n-1}) = -n^2 \frac{D_\varphi}{s_0^2} \delta\hat{g}_n + \frac{in}{(2\pi)^3 s_0}$$

$$\sum_{j=-\infty}^{\infty} \sum_{r=-\infty}^{\infty} \int \mathrm{d}^2 q \left( \delta\hat{g}_j(\boldsymbol{q},t)\hat{g}_r^{(0)}(\boldsymbol{k}-\boldsymbol{q},t) + \hat{g}_j^{(0)}(\boldsymbol{q},t)\delta\hat{g}_r(\boldsymbol{k}-\boldsymbol{q},t) \right) \tilde{K}_{n-j,r}(\boldsymbol{k}-\boldsymbol{q}). \quad (3.15)$$

The Fourier transform of the uniform distribution (3.9) reads

$$\hat{g}_n^{(0)}(\boldsymbol{k}) = (2\pi)^3 \, p^{(0)} \delta(\boldsymbol{k})\delta_{n,0} \,. \tag{3.16}$$

It is isotropic, i.e. it is invariant under rotations, and constant in time. Therefore, one can choose without loss of generality $\boldsymbol{k} = (k,0)$. Inserting (3.16) into (3.15) and using that the force $F_\varphi$ vanishes in the homogeneous, disordered state, yields an infinite dimensional system of linear differential equations:

$$\frac{\partial \delta\hat{g}_n(\boldsymbol{k},t)}{\partial t} = \sum_{r=-\infty}^{\infty} \left\{ \frac{iks_0}{2} (\delta_{n+1,r} + \delta_{n-1,r}) - n^2 \frac{D_\varphi}{s_0^2}\delta_{n,r} + \frac{inp^{(0)}}{s_0}\tilde{K}_{n,r}(\boldsymbol{k}) \right\} \delta\hat{g}_r(\boldsymbol{k},t) \,. \tag{3.17}$$

Hence, the stability of the spatially homogeneous, disordered state is determined by the eigenvalues of the matrix

$$\tilde{M}_{n,r} = \frac{iks_0}{2} (\delta_{n+1,r} + \delta_{n-1,r}) - n^2 \frac{D_\varphi}{s_0^2}\delta_{n,r} + \frac{inp^{(0)}}{s_0}\tilde{K}_{n,r}(\boldsymbol{k}) \,. \tag{3.18}$$

In order to calculate the eigenvalues numerically, it is necessary to find an appropriate closure of the infinite dimensional system of linear equations. Here we assume, that a critical $\tilde{n} > 0$ exists, such that $\delta\hat{g}_n = 0$ for $|n| > \tilde{n}$ holds (cf. [29]). That assumption is reasonable, because the $n$th Fourier coefficient is strongly damped, since

$$\frac{\partial \delta\hat{g}_n(\boldsymbol{k},t)}{\partial t} \propto -n^2 \frac{D_\varphi}{s_0^2} \, \delta\hat{g}_n(\boldsymbol{k},t) \,. \tag{3.19}$$

Using this approximation, the stability of the spatial homogeneous state can be studied. Please note, that only two approximations were used: First, correlations between particles are neglected (3.5) (mean-field); Second, the truncation of the hierarchy of equations (3.17). In principle, it is possible to analyze the stability for arbitrary wavenumbers $k = |\boldsymbol{k}|$, notably, there is no restriction to small $k$. Figure 3 shows the 15 largest eigenvalues for different parameters as a function of the wavenumber.

Unfortunately, the analysis discussed above does not supply any analytical criteria for the stability of the solution $p^{(0)}$, such as critical microscopic model parameters. Those will be derived in section 4 from the hydrodynamic theory. Besides, $p^{(0)}$ is the only solution to the Fokker-Planck equation known analytically, which stability one can investigate.

In this context, we would like to emphasize one difficulty which occurs if the focus is put on the dynamics of the lowest Fourier coefficients on large length scales, i.e. small wavenumbers $k$: The matrix elements $\tilde{K}_{n,r}(\boldsymbol{k})$ involve Bessel functions of the first kind of $k$ (see Appendix A and [29]) which are oscillating functions with alternating Taylor coefficients [30]. The approximation

$$J_{\nu,N}(x) \approx \sum_{m=0}^{N} \frac{(-1)^m}{m!\,\Gamma(m+\nu+1)} \left(\frac{x}{2}\right)^{2m+\nu} \tag{3.20}$$
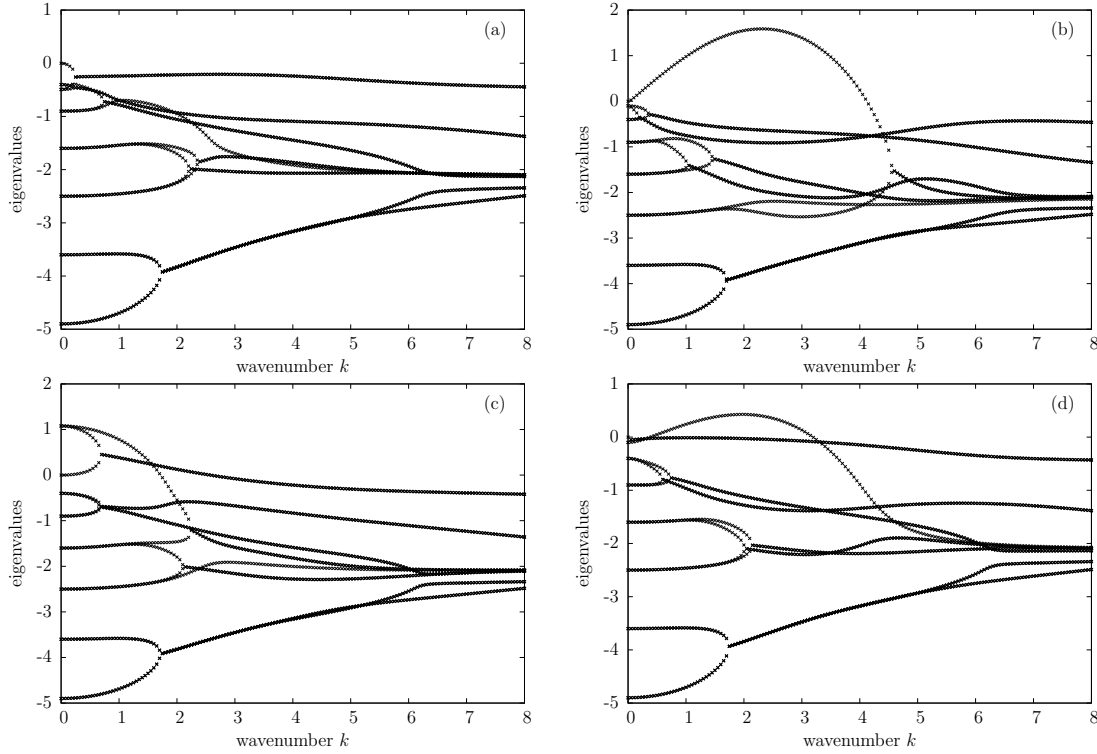
**Figure 3.** Eigenvalues of the truncated matrix $\tilde{M}_{n,r}$ (3.18) as a function of the wavenumber $k$. The 15 largest eigenvalues are shown, i.e $\tilde{n} = 7$ Fourier coefficients are considered. Different scenarios are distiguished: (a) $\mu_m = -2$, $\mu_a = -1$: the spatial homogeneous solution $p^{(0)}$ is stable; (b) $\mu_m = 5$, $\mu_a = 5$: long-wavelength instability; (c) $\mu_m = 2$, $\mu_a = -1$: homogeneous state ($k = 0$) becomes unstable first; (d) $\mu_m = -3$, $\mu_a = -3$: destabilization of a finite range $0 < k_{min} < k < k_{max}$ of wavenumbers. Other parameters: $D_\varphi = 0.1$, $\rho_0 = 1$, $\mu_r = 0$, $l_c = 0$, $l_s = 1$.

will only be valid in the vicinity of $x = 0$. For large $x$, $J_{\nu,N}(x)$ tends to either plus or minus infinity, but never to zero. This issue will be important for the derivation of hydrodynamic equations in the next section and is restricting their validity to small wavenumbers and large length scales, respectively.

## 4. Derivation of Hydrodynamic Equations

In this section, a hydrodynamic description of the many-particle system is derived directly from the one-particle FPE (3.8). For this purpose, it is convenient to work in Fourier space with respect to the angular variable $\varphi$. Both, the particle density $p(\boldsymbol{r}, \varphi, t)$ and the force $F_\varphi(\boldsymbol{r}, \varphi, t)$ (3.7) are $2\pi$-periodic functions in $\varphi$ and are therefore expanded in a Fourier series as follows:

$$p(\boldsymbol{r}, \varphi, t) \;\; = \frac{1}{2\pi} \sum_{n=-\infty}^{\infty} \hat{f}_n(\boldsymbol{r}, t)\, e^{-in\varphi} , \qquad\qquad (4.1a)$$

$$F_\varphi(\boldsymbol{r}, \varphi, t) = \frac{1}{2\pi} \sum_{n=-\infty}^{\infty} \hat{Q}_n(\boldsymbol{r}, t)\, e^{-in\varphi}. \tag{4.1b}$$

The Fokker-Planck equation in Fourier space is obtained by multiplying (3.8) with $e^{in\varphi}$ and integration over $\varphi \in [0, 2\pi]$:

$$\frac{\partial \hat{f}_n}{\partial t} + s_0 \left( \nabla \hat{f}_{n-1} + \nabla^* \hat{f}_{n+1} \right) = \frac{1}{2\pi} \frac{in}{s_0} \sum_{j=-\infty}^{\infty} \hat{f}_j\, \hat{Q}_{n-j} - n^2 \frac{D_\varphi}{s_0^2} \hat{f}_n. \tag{4.2}$$

In (4.2), the complex derivative $\nabla = 0.5\,(\partial_x + i\partial_y)$ was introduced. The Fourier coefficients

$$\hat{f}_n(\boldsymbol{r}, t) = \int_0^{2\pi} \mathrm{d}\varphi\, p(\boldsymbol{r}, \varphi, t) e^{in\varphi} = \rho(\boldsymbol{r}, t) \left\langle e^{in\varphi} \right\rangle \tag{4.3}$$

obey the symmetry $\hat{f}_n^*(\boldsymbol{r}, t) = \hat{f}_{-n}(\boldsymbol{r}, t)$, since $p(\boldsymbol{r}, \varphi, t)$ is real-valued. The lowest Fourier coefficients are related to macroscopic physical quantities, namely the marginal particle density $\rho(\boldsymbol{r}, t)$ and also the momentum field $\boldsymbol{w}(\boldsymbol{r}, t) = (w_x, w_y)$ via

$$\rho(\boldsymbol{r}, t) = \hat{f}_0(\boldsymbol{r}, t), \tag{4.4a}$$

$$w_x(\boldsymbol{r}, t) = \frac{s_0}{2} \left( \hat{f}_1(\boldsymbol{r}, t) + \hat{f}_{-1}(\boldsymbol{r}, t) \right), \tag{4.4b}$$

$$w_y(\boldsymbol{r}, t) = \frac{s_0}{2i} \left( \hat{f}_1(\boldsymbol{r}, t) - \hat{f}_{-1}(\boldsymbol{r}, t) \right). \tag{4.4c}$$

The symmetric temperature tensor

$$\hat{T} = \begin{pmatrix} \langle \cos\varphi^2 \rangle - \langle \cos\varphi \rangle^2 & \langle \sin\varphi \cos\varphi \rangle - \langle \sin\varphi \rangle \langle \cos\varphi \rangle \\ \langle \sin\varphi \cos\varphi \rangle - \langle \sin\varphi \rangle \langle \cos\varphi \rangle & \langle \sin\varphi^2 \rangle - \langle \sin\varphi \rangle^2 \end{pmatrix} \tag{4.5}$$

as defined in [23, 25, 28], is basically related to the second Fourier coefficients:

$$T_{xx} = \frac{1}{2} \left( 1 + \frac{\hat{f}_2(\boldsymbol{r}, t) + \hat{f}_{-2}(\boldsymbol{r}, t)}{2\rho(\boldsymbol{r}, t)} \right) - \left( \frac{\hat{f}_1(\boldsymbol{r}, t) + \hat{f}_{-1}(\boldsymbol{r}, t)}{2\rho(\boldsymbol{r}, t)} \right)^2, \tag{4.6a}$$

$$T_{xy} = \frac{\hat{f}_2(\boldsymbol{r}, t) - \hat{f}_{-2}(\boldsymbol{r}, t)}{4i\rho(\boldsymbol{r}, t)} - \frac{\left( \hat{f}_1(\boldsymbol{r}, t) \right)^2 - \left( \hat{f}_{-1}(\boldsymbol{r}, t) \right)^2}{4i\,(\rho(\boldsymbol{r}, t))^2}, \tag{4.6b}$$

$$T_{yy} = \frac{1}{2} \left( 1 - \frac{\hat{f}_2(\boldsymbol{r}, t) + \hat{f}_{-2}(\boldsymbol{r}, t)}{2\rho(\boldsymbol{r}, t)} \right) + \left( \frac{\hat{f}_1(\boldsymbol{r}, t) - \hat{f}_{-1}(\boldsymbol{r}, t)}{2\rho(\boldsymbol{r}, t)} \right)^2. \tag{4.6c}$$

In the following, the behaviour of these quantities is deduced from (4.2). Therefore, the Fourier coefficients of the force $\hat{Q}_n(\boldsymbol{r}, t)$ are approximately calculated by expanding $p(\boldsymbol{r} + \boldsymbol{r}_{ji}, \varphi, t)$ into a multidimensional Taylor series for small $|\boldsymbol{r}_{ji}|$ [31], substituting (4.1a) into (3.7) and evaluating the remaining integral. Here, we consider all terms up to the third order of the Taylor expansion. This approximation holds for spatially slowly varying densities, i.e. large system size compared to the interaction radius $l_s$.

Again, the Fokker-Planck equation turns into an infinite hierarchy of equations (4.2) in Fourier space. An appropriate closure scheme is used in order to consider only the first Fourier coefficients. Close to the order-disorder transition, the mean speed of

the system is small, i.e. $|\boldsymbol{w}|/(s_0\rho) \propto \epsilon$, where $\epsilon$ is a small number. Furthermore, the dynamics of the Fourier coefficients (4.2) suggests, that $\hat{f}_1$ is larger than $\hat{f}_k$ with $|k| > 1$, because of the damping term in (4.2) proportional to $k^2$, leading to the scaling relations

$$\nabla \propto \epsilon, \quad \partial_t \propto \epsilon, \quad \hat{f}_k \propto \epsilon^{|k|}. \tag{4.7}$$

In [20] it is argued, that the scaling ansatz of the temporal and spatial derivatives reflects the propagating nature of the system. This closure scheme described above was already used in [17, 20, 22, 31] and in [21] in an analogous way for nematic particles. A system of three nonlinear partial differential equations is obtained by keeping all terms up to the order $\epsilon^3$.

$$\frac{\partial \rho}{\partial t} = -s_0 \left( \nabla \hat{f}_1^* + \nabla^* \hat{f}_1 \right) \tag{4.8a}$$

$$\begin{aligned}
\frac{\partial \hat{f}_1}{\partial t} &= (\xi_1 \rho - \xi_5) \hat{f}_1 - \xi_1 \hat{f}_2 \hat{f}_1^* + \left( \xi_2 - \frac{32}{9} \xi_3 \right) \hat{f}_2 \nabla^* \rho + \left( \frac{32}{45} \xi_3 \rho - s_0 \right) \nabla^* \hat{f}_2 \\
&\quad + \left( \frac{32}{9} \xi_3 \rho - \xi_2 \rho - s_0 \right) \nabla \rho - \frac{64}{45} \xi_3 \hat{f}_1^* \nabla \hat{f}_1 \\
&\quad + \frac{\xi_4}{2} \left[ \rho \left( \Delta \hat{f}_1 + 2 \nabla^2 \hat{f}_1^* \right) - 2 \hat{f}_1^* \nabla^2 \rho \right] + (\xi_7 - \xi_6) \nabla^* (\nabla^2 \rho)
\end{aligned} \tag{4.8b}$$

$$\frac{\partial \hat{f}_2}{\partial t} = 2 \left[ -2\xi_5 \hat{f}_2 + \xi_1 \hat{f}_1^2 - \left( \frac{s_0}{2} + \frac{64}{45} \xi_3 \rho \right) \nabla \hat{f}_1 + \left( \frac{32}{9} \xi_3 - \xi_2 \right) \hat{f}_1 \nabla \rho - \xi_4 \rho \nabla^2 \rho \right] \tag{4.8c}$$

The following coefficients are introduced:

$$\xi_1 = \frac{\pi}{4} \int_{l_c}^{l_s} \mathrm{d}r_{ji} \, r_{ji} \left[ \mu_m(r_{ji}) - \mu_a(r_{ji}) \right], \tag{4.9a}$$

$$\xi_2 = \frac{\pi}{s_0} \int_0^{l_c} \mathrm{d}r_{ji} \, r_{ji}^2 \, \mu_r(r_{ji}), \tag{4.9b}$$

$$\xi_3 = \frac{1}{\pi} \int_{l_c}^{l_s} \mathrm{d}r_{ji} \, r_{ji}^2 \left[ \mu_m(r_{ji}) + \mu_a(r_{ji}) \right], \tag{4.9c}$$

$$\xi_4 = \frac{\pi}{8} \int_{l_c}^{l_s} \mathrm{d}r_{ji} \, r_{ji}^3 \left[ \mu_m(r_{ji}) - \mu_a(r_{ji}) \right], \tag{4.9d}$$

$$\xi_5 = \frac{D_\varphi}{s_0^2}, \tag{4.9e}$$

$$\xi_6 = \frac{\pi}{2s_0} \int_0^{l_c} \mathrm{d}r_{ji} \, r_{ji}^4 \, \mu_r(r_{ji}), \tag{4.9f}$$

$$\xi_7 = \frac{16}{9\pi} \int_{l_c}^{l_s} \mathrm{d}r_{ji} \, r_{ji}^4 \left[ \mu_m(r_{ji}) + \mu_a(r_{ji}) \right]. \tag{4.9g}$$

Equation (4.8a) is simply the continuity equation representing the conservation of the particle number $N$.

### 4.1. Hydrodynamic Limit

Another simplification of the system (4.8) is reached by adiabatically eliminating $\hat{f}_2$, i.e. $\partial_t \hat{f}_2 \approx 0$, where

$$\hat{f}_2 \approx \frac{1}{2\xi_5}\left[\xi_1 \hat{f}_1^2 - \left(\frac{s_0}{2} + \frac{64}{45}\xi_3 \rho\right)\nabla \hat{f}_1 + \left(\frac{32}{9}\xi_3 - \xi_2\right)\hat{f}_1 \nabla \rho - \xi_4 \rho \nabla^2 \rho\right] \tag{4.10}$$

follows. Please note, that $\xi_5 \propto D_\varphi > 0$ was assumed. By identifying Fourier coefficients with physical quantities (4.4), familiar hydrodynamic equations are obtained.

$$\frac{\partial \rho}{\partial t} = -\nabla \cdot \boldsymbol{w} \tag{4.11a}$$

$$\frac{\partial \boldsymbol{w}}{\partial t} = \left(\lambda_1 - \eta_1 |\boldsymbol{w}|^2\right)\boldsymbol{w} + \lambda_2 \nabla \rho + \lambda_3 \nabla(\Delta \rho) + \lambda_4 \Delta \boldsymbol{w} + \lambda_5 \nabla \cdot (\nabla \cdot \boldsymbol{w}) + \eta_2 (\boldsymbol{w} \cdot \nabla) \cdot \boldsymbol{w}$$

$$+ \eta_3 \left(\frac{1}{2}\nabla |\boldsymbol{w}|^2 - \boldsymbol{w} \cdot (\nabla \cdot \boldsymbol{w})\right) + \eta_4 (\boldsymbol{w} \cdot \nabla) \cdot \nabla \rho + \eta_5 \boldsymbol{w} \cdot \Delta \rho + \eta_6 \boldsymbol{w} \cdot ((\boldsymbol{w} \cdot \nabla)\rho)$$

$$+ \gamma_1 \boldsymbol{w} \cdot (\nabla \rho)^2 + \gamma_2 (\nabla \cdot \boldsymbol{w}) \cdot \nabla \rho + \gamma_3 \hat{A}_w \cdot \nabla \rho + \gamma_4 \hat{M}_w \cdot \nabla \rho$$

$$+ \gamma_5 \left[2(\nabla \rho \cdot \nabla) \cdot \nabla \rho - (\Delta \rho) \cdot \nabla \rho\right] \tag{4.11b}$$

Here, the matrices

$$\hat{M}_w = \begin{pmatrix} \partial_x w_x & \frac{1}{2}\left(\partial_y w_x + \partial_x w_y\right) \\ \frac{1}{2}\left(\partial_y w_x + \partial_x w_y\right) & \partial_y w_y \end{pmatrix}, \tag{4.12a}$$

$$\hat{A}_w = \begin{pmatrix} 0 & \partial_x w_y - \partial_y w_x \\ \partial_y w_x - \partial_x w_y & 0 \end{pmatrix} \tag{4.12b}$$

were introduced. The transport coefficients $\{\lambda_i, \eta_i, \gamma_i\}$ (B.1) as functions of $\xi_i$ (4.9) are listed in Appendix B. The hydrodynamic equations (4.11) are comparable in structure to the theory of Toner and Tu [13,14] but contains additional gradient terms comparable to [19].

Let us begin the analysis by neglecting the spatial derivatives in (4.11) and analyzing the fixed points of

$$\frac{d\boldsymbol{w}}{dt} = \left(\lambda_1 - \eta_1 |\boldsymbol{w}|^2\right)\boldsymbol{w}. \tag{4.13}$$

Apparently, two spatially homogeneous solutions exist: First, $\boldsymbol{w}_0 = 0$ corresponding to a disordered phase and vanishing center of mass velocity. Second,

$$\boldsymbol{w}_1 = \sqrt{\frac{\lambda_1}{\eta_1}}\,\boldsymbol{e}, \tag{4.14}$$

where $\boldsymbol{e}$ denotes an arbitrary unit vector reflecting the isotropy of the system. For $\lambda_1 < 0$, only the fixed point $\boldsymbol{w}_0$ exists and is stable against spatially homogeneous perturbations. For $\lambda_1 \geq 0$, $\boldsymbol{w}_1$ is a second fixed point corresponding to an ordered phase with nonzero mean-speed (swarming phase). Please note, that $\eta_1$ is always positive. In $\lambda_1 = 0$, i.e.

$$\int_{l_c}^{l_s} dr_{ji}\, r_{ji}\left(\mu_m(r_{ji}) - \mu_a(r_{ji})\right) = \frac{4D_\varphi}{\pi \rho_0 s_0^2}, \tag{4.15}$$

the system undergoes a supercritical pitchfork bifurcation. By introducing the effective coupling strength

$$\mu = \int_{l_c}^{l_s} \mathrm{d}r_{ji}\, r_{ji} \left( \mu_m(r_{ji}) - \mu_a(r_{ji}) \right) \tag{4.16}$$

together with the critical coupling parameter

$$\mu_c = \frac{4D_\varphi}{\pi \rho_0 s_0^2} \tag{4.17}$$

one can rewrite (4.14) close to the critical point $0 < \mu - \mu_c \ll \mu_c$ in the leading order as follows

$$|\boldsymbol{w}_1| \simeq s_0 \rho_0 \left( \frac{\mu - \mu_c}{\mu_c} \right)^\beta , \tag{4.18}$$

where one can read off the mean-field exponent $\beta = 1/2$. Hence, the order-disorder transition is continuous in the mean-field analysis.

Equation (4.15) defines the transition line in the $(\mu_m, \mu_a)$-parameter space. Interestingly, only the integrated interaction-strengths are important, the exact functional dependence on the distance between two particles $\mu_{m,a} = \mu_{m,a}(r_{ji})$ does not matter. Furthermore, collective motion is possible in both situations, pure attraction to particles moving away (pursuit: $\mu_m > 0$, $\mu_a = 0$) and pure repulsion from approaching particles (escape: $\mu_m = 0$, $\mu_a < 0$), respectively.

Up to now, only the spatial homogeneous system was analyzed. In the following, the stability of the disordered, homogeneous solution $\boldsymbol{w}_0 = 0$ against spatial perturbations is considered. In order to investigate the stability of $\boldsymbol{w}_0$, the ansatz

$$\rho(\boldsymbol{r}, t) = \rho_0 + \delta\rho(\boldsymbol{r}, t) , \tag{4.19a}$$

$$\boldsymbol{w}(\boldsymbol{r}, t) = \delta\boldsymbol{w}(\boldsymbol{r}, t) \tag{4.19b}$$

is inserted in (4.11) and the resulting equations are linearized in the perturbations which are assumed to be small. The linearized equations read

$$\frac{\partial \delta\rho}{\partial t} = -\nabla \cdot \delta\boldsymbol{w} , \tag{4.20a}$$

$$\frac{\partial \delta\boldsymbol{w}}{\partial t} = \lambda_1 \delta\boldsymbol{w} + \lambda_2 \nabla\delta\rho + \lambda_3 \nabla(\Delta\delta\rho) + \lambda_4 \Delta\delta\boldsymbol{w} + \lambda_5 \nabla \cdot (\nabla \cdot \delta\boldsymbol{w}) . \tag{4.20b}$$

Inserting the exponential ansatz

$$\delta\rho(\boldsymbol{r}, t) = \zeta_\rho \exp\left( \sigma t + i\boldsymbol{k}\boldsymbol{r} \right) , \tag{4.21a}$$

$$\delta\boldsymbol{w}(\boldsymbol{r}, t) = \boldsymbol{\zeta_w} \exp\left( \sigma t + i\boldsymbol{k}\boldsymbol{r} \right) \tag{4.21b}$$

yields the growth rate $\sigma$ depending on the wavenumber $k = |\boldsymbol{k}|$:

$$\sigma_1 = \lambda_1 - \lambda_4 k^2 , \tag{4.22a}$$

$$\sigma_{2,3} = \frac{1}{2} \left[ \lambda_1 - (\lambda_4 + \lambda_5) k^2 \pm \sqrt{[\lambda_1 - (\lambda_4 + \lambda_5) k^2]^2 + 4k^2 (\lambda_2 - \lambda_3 k^2)} \right] . \tag{4.22b}$$

Provided all eigenvalues are less than zero, the disordered spatially homogeneous state is stable. The first eigenvalue $\sigma_1$ is equal to $\lambda_1$ for $k = 0$, i.e. the stability of $\boldsymbol{w}_0$ is

determined by the sign of $\lambda_1$. That is the destabilisation of the homogeneous state as discussed before. For $\lambda_4 > 0$, the first eigenvalue $\sigma_1$ is monotonically decreasing. However, the eigenvalue $\sigma_1$ is monotonically increasing for $\lambda_4 < 0$. In this case, the hydrodynamic equations (4.11) loose their validity. This unphysical behaviour is due to the restriction to third derivatives when the integral (3.7) was calculated. Furthermore, it is problematically that the Taylor coefficients have alternating signs so that Taylor polynomials converge slowly as argued at the end of section 3.1. To predict the behaviour of the system in that case, one needs to consider higher order terms. Unfortunately, the number of terms that has to be considered to be consistent with the scaling ansatz (4.7), grows rapidly.

Nevertheless, it is possible to predict the stability of $\boldsymbol{w}_0$ by analyzing those eigenvalues, which tend to zero for small wavenumbers (hydrodynamic modes [14]). For small wavenumbers, the eigenvalue $\sigma_2$ is expanded in a Taylor series:

$$\sigma_2 \simeq -\frac{\lambda_2}{\lambda_1} k^2 + \frac{\lambda_2^2 + \lambda_1^2 \lambda_3 - \lambda_1 \lambda_2 (\lambda_4 + \lambda_5)}{\lambda_1^3} k^4 + \mathcal{O}(k^6). \tag{4.23}$$

Suppose, $\boldsymbol{w}_0$ is stable against spatially homogeneous pertubations, i.e. $\lambda_1 < 0$. In that case, $\boldsymbol{w}_0$ will become unstable, if $\lambda_2 > 0$. Considering (4.11), this instability is reasonable: for $\lambda_2 > 0$, inhomogeneities in the particle density will lead to a flow in the direction of the density gradients while for $\lambda_2 < 0$ density inhomogeneities decay due to inverse flows. The amplification of density gradients will lead to an agglomeration of particles (cf. figure 2E). This hypothesis is supported by numerical simulations of the microscopic model, as shown in the next section and in [28]. A similar instability due to the gradient term in (4.11) is also known from other active matter systems [22, 32]. The critical line is given by $\lambda_2 = 0$, i.e.

$$\int_{l_c}^{l_s} \mathrm{d}r_{ji}\, r_{ji}^2 \left(\mu_m(r_{ji}) + \mu_a(r_{ji})\right) = \frac{9\pi}{16 s_0 \rho_0} \left(\frac{s_0^2}{2} + \frac{\rho_0 \pi}{2} \int_0^{l_c} \mathrm{d}r_{ji}\, r_{ji}^2 \mu_r(r_{ji})\right). \tag{4.24}$$

The stability analysis of the ordered state $\boldsymbol{w}_1$ using the full hydrodynamic equations is much more demanding. It is shown in [17] that a long wavelength instability can occur in the ordered regime. Furthermore, giant number fluctuations are expected to emerge because of the structure of the equations (4.11) [15, 16].

Finally, the prediction of the hydrodynamic theory derived in this section is compared to the predictions of the stability analysis using the kinetic description in section 3.1. Figure 4 shows the eigenvalue spectrum by the two theories, whereby the hydrodynamic description (4.11) can be understood as an approximation to the full system (3.11). The hydrodynamic theory describes the dynamics of the many-particle system on large length scales and small wavenumbers, respectively. Thus, the eigenvalues coincide in the limit $k \to 0$. For large $k$, deviations occur due to the approximations made, namely:

- restriction to third derivatives;
- scaling ansatz and closure scheme (4.7);
- restriction to the lowest Fourier coefficients.
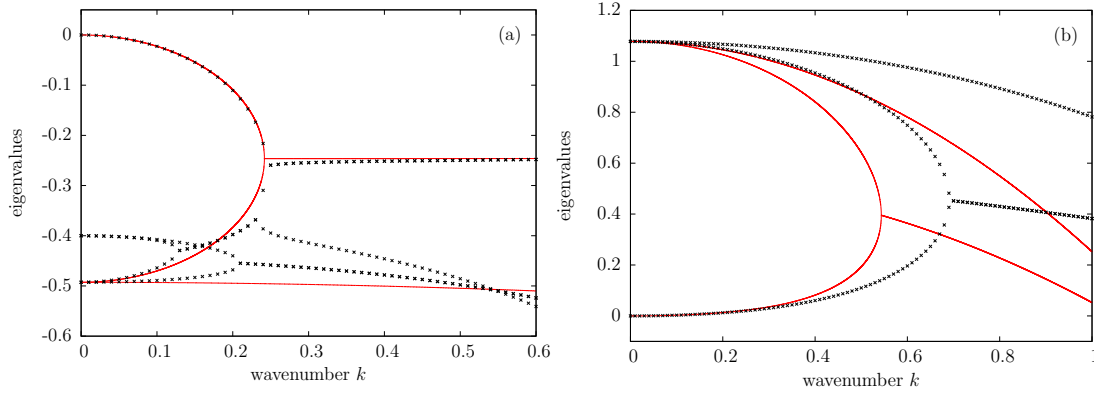
**Figure 4.** Eigenvalues as predicted by the hydrodynamic theory (4.11) (red lines) and the kinetic description (3.11) (black crosses) which determine the stability of the disordered, spatially homogeneous state: $p^{(0)} = \rho_0/(2\pi)$; $\rho(\boldsymbol{r}, t) = \rho_0 = N/L^2$; $\boldsymbol{w} = \boldsymbol{w}_0 = 0$. For small wavenumbers $k \to 0$, the eigenvalues coincide, i.e. the hydrodynamic theory is valid on large length scales. Parameters: (a) $\mu_m = -2$, $\mu_a = -1$; (b): $\mu_m = 2$, $\mu_a = -1$; $D_\varphi = 0.1$, $\rho_0 = 1$, $\mu_r = 0$, $l_c = 0$, $l_s = 1$.

Nevertheless, the hydrodynamic theory yields important insigths on the macroscopic behaviour of the system. The symmetry breaking, i.e. the existence of an collective motion mode is predicted. Moreover, the stability of the homogeneous solutions to the hydrodynamic equations can be analyzed both analytically and numerically. Finally, it allows to obtain analytical results on the order-disorder transition line as well as the occurrence of clustering.

## 5. Comparison with Numerical Simulations

In order to analyze the stability of the disordered, homogeneous state, we have performed systematic numerical simulations of the individual-based model (2.1). The degree of collective motion was measured using the time averaged polar order parameter

$$\langle \Phi \rangle_t = \left\langle \left\| \frac{1}{N s_0} \sum_{i=1}^{N} \boldsymbol{v}_i(t) \right\| \right\rangle_t . \tag{5.1}$$

Here $\langle \cdot \rangle_t$ represents a temporal average. $\langle \Phi \rangle_t = 1$ corresponds to perfect orientational order with all agents moving in the same direction, whereas a vanishing $\langle \Phi \rangle_t$ corresponds to a completely disordered system. Please note that $\langle \Phi \rangle_t = 0$ can only be observed in the thermodynamic limit ($N \to \infty$). In a finite, disordered system we will measure a small, but finite $\langle \Phi \rangle_t \gtrsim 0$ due to finite size fluctuations of the order $1/\sqrt{N}$.

In order to measure the deviations from a homogeneous state, we have subdivided the simulation domain into square cells of size $l_s \times l_s$ set by the sensory range. We used this spatial subdivision to calculate the spatial entropy function

$$S = - \sum_{j, n_j \neq 0} p_j \log p_j = - \sum_{j, n_j \neq 0} \frac{n_j}{N} \log \frac{n_j}{N}, \tag{5.2}$$

where the summation occurs over all occupied cells of the grid with $n_j \geq 1$ ($n_j$ is the number of particles in the $j$ths cell). This allows us to define the following spatial order parameter

$$\langle \Psi \rangle_t = \left\langle 1 - \frac{S}{S_{max}} \right\rangle_t \tag{5.3}$$

with $S_{max}$ being the maximal value of the spatial entropy corresponding to a homogeneous distribution of particles. $\langle \Psi \rangle_t = 0$ corresponds to a perfectly disordered state, whereas $\langle \Psi \rangle_t > 0$ indicates a spatially inhomogeneous distribution of particles (clusters, bands), where $\langle \Psi \rangle_t = 1$ corresponds to the extreme situation where all particles are located in a single cell.
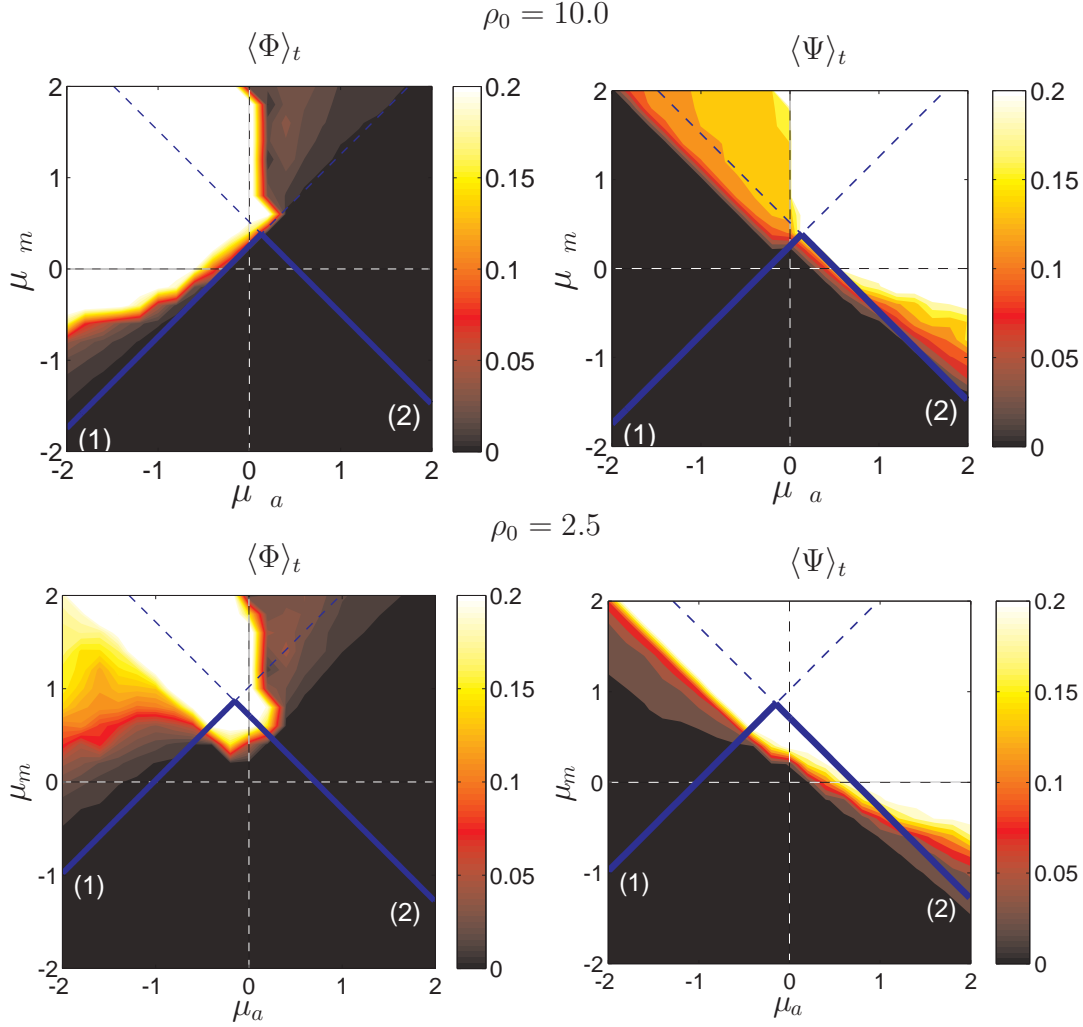
In order to test the stability of the disordered state, we have averaged the two order parameters over a time interval $\Delta t = 1000$ after an initial time $t_{ini} = 1000$. Please note, that for certain parameter values it is possible that the system has not reached a stationary state after $t = 1000$. However, this initial time is sufficient to account for deviations from the homogeneous disordered state, which we are interested in. Accordingly, we are not interested in the actual stationary values of $\langle \Phi \rangle_t$ and $\langle \Psi \rangle_t$. Thus, we set the upper limit of the colour bar for both order parameters in figures 5 and 6 to 0.2. In consequence, all regions of parameter space, where $\langle \Phi \rangle_t \geq 0.2$ or $\langle \Psi \rangle_t \geq 0.2$ will appear white in figures 5 & 6.

The stochastic differential equations of the microscopic model were integrated with periodic boundary conditions using the stochastic version of the Euler algorithm with a numerical time step $dt = 0.01$. The initial condition for all simulations was the disordered, spatially homogeneous state.

For simplicity, we consider only constant interaction strengths (independent of the distance): $\mu_{m,a}(r_{ji}) = \mu_{m,a} = const$. Here, we focus on the analysis of the stability of the disordered, homogeneous solution with respect to variations of the interaction parameters $\mu_a$ and $\mu_m$. The analytical predictions of the hydrodynamic theory for the onset of instability of the disordered solution are represented by two intersecting critical lines in the $(\mu_a, \mu_m)$-plane perpendicular to each other (figure 5). The first one ($\mu_a \sim \mu_m$) corresponds to the orientational instability and onset of collective motion, cf. (4.15) and line (1) in figure 5, whereas the second one ($\mu_a \sim -\mu_m$) corresponds to the density instability associated with structure formation due to effective attraction between particles, cf. (4.24) and line (2) in figure 5. The homogeneous, disordered solution is predicted to be linearly stable only "below" both critical lines.

The emergence of collective motion as well as the destabilization of the homogeneous density distribution is mostly confirmed by the numerical individual-based simulations. In specific parameter regions, deviations from the hydrodynamic theory are observed.

In particular, we observe a high degree of collective motion in the escape and pursuit region and strong deviations from the homogeneous spatial distribution of particles in the pure attraction regime as well as in the escape-pursuit regime (in particular in the pursuit dominated regime for $|\mu_m| > |\mu_a|$). This also confirms our previous results of comprehensive numerical investigations of related individual-based models [28, 33].

**Figure 5.** Comparison of numerical simulations of the individual-based model with the predictions of the hydrodynamic theory on the stability of the disordered solution in the $(\mu_m, \mu_a)$-plane for different densities: $\rho_0 = 10.0$ ($L = 20$, top) and $\rho_0 = 2.5$ ($L = 40$, bottom). **Left:** Average orientational order parameter $\langle \Phi \rangle_t$; **Right:** Average spatial inhomogeneity order parameter $\langle \Psi \rangle_t$. The solid blue (gray) lines show the critical lines for the instability of the disordered solution. Line (1) corresponding to the orientation instability (4.15), whereas line (2) corresponds to the clustering instability (4.24). Other parameters: $D_\varphi = 0.06$, $N = 4000$, $\mu_r = 5$, $l_c = 0.2$, $l_s = 1$, $s_0 = 0.25$, $dt = 0.01$.

Disagreements between simulations and the theoretical prediction (non-vanishing orientational order and/or clustering in simulations below the two critical lines) appear predominantly close to the intersection of the two critical lines and are stronger at low densities. They might be associated with the mean-field assumptions used in order to derive the hydrodynamic theory. On the one hand, at low densities the assumption of a continuous density of neighbours is strongly violated. On the other hand, correlations between particles may play an important role in the respective parameter range (likewise for high densities). Thus, the factorization of the N-particle PDF into a product of one-
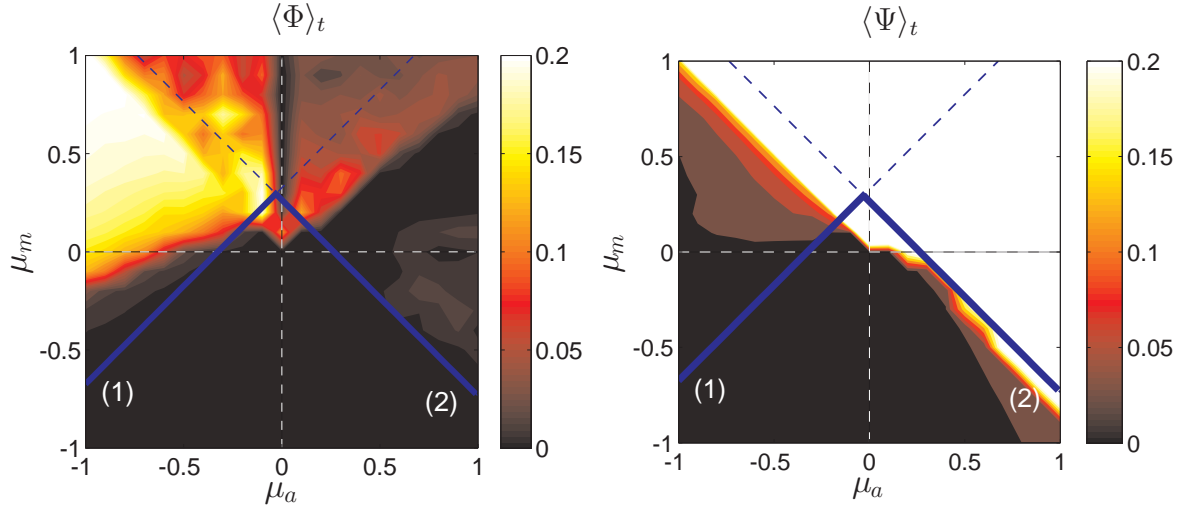
**Figure 6.** Results of numerical simulations on the stability of the disordered solution in the $(\mu_m, \mu_a)$-plane for vanishing short-ranged repulsion $(l_c = 0)$. The spatial order parameter $\langle \Psi \rangle_t$ shows emergence of structures below the critical line (2). Other parameters: $N = 4000$, $l_s = 1$, $s_0 = 0.25$, $D_\varphi = 0.02$, $L = 40$.

particle PDFs (3.5) leads to a questionable approximation in that case.

Another possible explanation for disagreement between theory and simulation is a breakdown of the homogeneous, disordered solution due to finite amplitude instabilities at parameters where this solution is still linearly stable.

For weak (or vanishing) short-ranged repulsion $(l_s \gg l_c$ or $\mu_r \ll |\mu_{m,a}|)$, we observe inhomogeneous states without polar order far in the head-on-head regime $(\mu_m < 0$, $\mu_a > 0)$, clearly below the critical line predicted by the hydrodynamic theory as shown in figure 6. This instability was missed in the previous study of the model [28]. We were able to confirm it, using our kinetic approach (see section 3) by positive eigenvalues of the matrix determining the stability of the disordered solution at the respective parameter values. A close inspection of the dynamics of the individual-based model in this parameter region reveals the emergence of dense nematic filaments with particles moving in an anti-parallel fashion within the filament, whereby approximately half of the particles moves in either direction along the filament (see figure 7).

The hydrodynamic theory derived in section 4 is not able to account for this kind of structures as it considers only the (polar) momentum field and not the nematic director field as a coarse-grained variable. An extension of the hydrodynamic theory by including an equation for the nematic director field may allow for identifying instabilities due to the onset of nematic order, however it goes beyond the scope of this work. We refer the reader to some recent theoretical works on active nematics [21, 34–37].
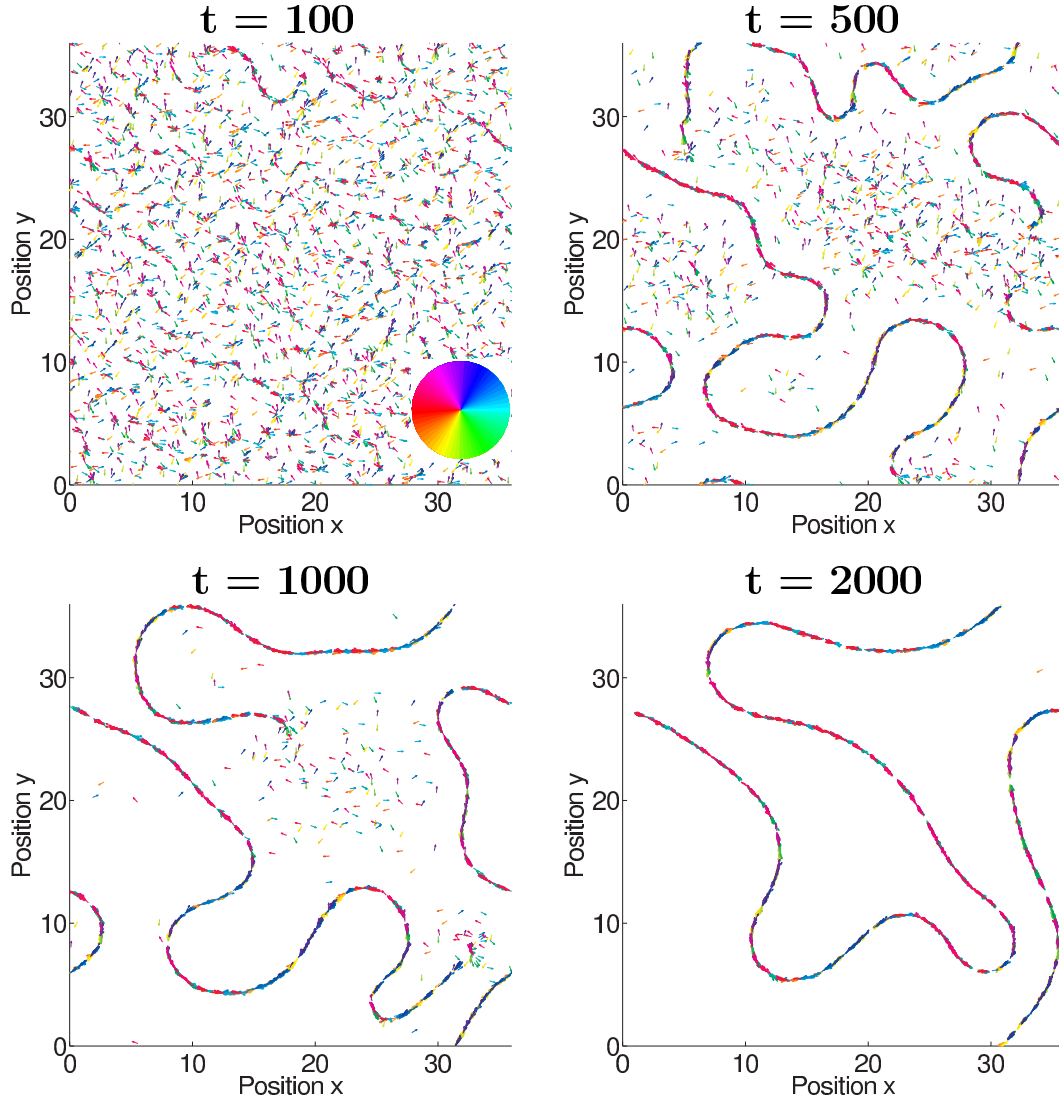
**Figure 7.** A sequence of snapshots of one simulation for different times visualizing the formation of nematic filaments for $\mu_a = 0.6$, $\mu_m = -0.4$. Other parameters: $N = 4000$, $l_s = 1$, $s_0 = 0.25$, $D_\varphi = 0.02$, $L = 36$.

## 6. Discussion

In this work, we have derived and analyzed a kinetic and hydrodynamic description of self-propelled particles with selective attraction-repulsion interaction.

At first, we derived a kinetic description of the system based on the Fourier transform of the probability density function. The corresponding system of equations for the successive Fourier modes can be used for efficient numerical analysis of the linear stability of solutions of the nonlinear Fokker-Planck equation. We have analyzed the stability of the disordered, spatially homogeneous solution. In addition, we have shown that the integration over the social forces yields Bessel functions of the first kind, which enter the matrix elements of the corresponding linearized system of differential equations

in Fourier space. Due to the alternating Taylor coefficients of the corresponding Bessel functions, a closure approximation, corresponding to a finite order expansion, immediately leads to unphysical divergences at large wavenumbers $k$.

Furthermore, we have derived a hydrodynamic theory by truncating the "small-wavenumber-expansion" at the third order. The resulting hydrodynamic equations are in agreement with the generic Toner and Tu theory of active matter but contains additional gradient terms due to the selective attraction-repulsion interaction. Our work establishes a direct link between the microscopic parameters of the individual-based model and the macroscopic parameters governing the behaviour of the coarse-grained hydrodynamic variables (density and momentum fields). A comparison between the eigenvalues obtained from hydrodynamic theory and the kinetic description, which takes higher orders into account, allows us to assess the validity of the hydrodynamic theory.

We performed extensive simulations of the microscopic model based on stochastic differential equations focusing on the $(\mu_m, \mu_a)$-plane in the parameter space. The critical lines obtained from the hydrodynamic theory, where the disordered, spatially homogeneous solution becomes unstable, show good agreement with the numerical results at sufficiently high densities. However, at certain parameters clear deviations appear, as for example in the vicinity of the crossing of the two critical lines at low densities.

This leads us to the important question of the validity of the approximations made in order to derive the coarse-grained theory. One common assumption is that of molecular chaos, which allows to factorize the N-particle PDF into a product of N one-particle PDFs. In models with collision-like interactions, the approximation is supposed to work best at low densities, where the mean-free path of particles between interactions is large [17, 19]. However, in our case, we observe large deviations at low densities. This contradicting effect may be due to an approximation required to evaluate the integrals over the social forces. It relies on a Taylor expansion of the one-particle density function around the position of a focal individual. Thus $p(\boldsymbol{r}, \varphi, t)$ is assumed to be continuous and differentiable, an assumption which is likely to be violated at low densities. Similar arguments have been put forward also in [22]. The impact of individual (angular) noise on the mean-field assumption may also be not straight forward. Intuitively, one would argue that uncorrelated individual noise terms always decrease correlations between interacting particles. However, for self-propelled particles, angular noise leads to a stronger localization of particles [38, 39], thus in principle also to a prolonged interaction between neighbours, which may in principle enhance multi-particle correlations.

Furthermore, the systematic comparison of the numerical results with the analytical prediction revealed an unexpected additional instability. It corresponds to the emergence of filamentous structures with nematic order. Onset of nematic order is linked to the dynamics of the second Fourier amplitude, which was adiabatically eliminated in order to derive the hydrodynamic theory. Thus, the hydrodynamic theory cannot account for this instability, but we were able to confirm it by numerical evaluation of

the linearized kinetic equations derived in section 3.

So far, hydrodynamic equations of active matter were derived directly from minimal microscopic models of self-propelled particles with velocity-alignment. Here, we show that it is also possible to derive such equations for a more complex model of self-propelled particles with selective attraction-repulsion interaction and establish a direct link between the microscopic and macroscopic level of description. The model exhibits a large variety of different phases. Thus we believe, it might be not only of interest from the biological point of view, as an alternative to models including explicit alignment of individual agents, but offers also interesting playground for the study of self-organization, pattern formation and phase transitions at far-from-equilibrium conditions.

## Appendix A. Calculation of $\tilde{K}_{p,n}$ (3.13)

In this section, it is sketched, how the matrix elements $\tilde{K}_{p,n}(\boldsymbol{k})$, defined by

$$\hat{K}_p(\boldsymbol{k}, t) = \int \mathrm{d}^2 r \int_0^{2\pi} \mathrm{d}\varphi\, F(\boldsymbol{r}, \varphi, t) e^{i\boldsymbol{k}\boldsymbol{r} + ip\varphi}, \tag{A.1a}$$

$$\hat{K}_p(\boldsymbol{k}, t) = \sum_{r=-\infty}^{\infty} \tilde{K}_{p,r}(\boldsymbol{k}) \hat{g}_r(\boldsymbol{k}, t) \tag{A.1b}$$

and used for the stability analysis of the spatial homogeneous, disordered solution (3.9) of the Fokker-Planck equation (3.8) in section 3.1, are calculated. $\tilde{K}_{p,n}$ is obtained by inserting the inverse Fourier transform of the one-particle PDF

$$p(\boldsymbol{r}, \varphi, t) = \frac{1}{(2\pi)^3} \sum_{n=-\infty}^{\infty} \int \mathrm{d}^2 k\, \hat{g}_n(\boldsymbol{k}, t) e^{-i\boldsymbol{k}\boldsymbol{r} - in\varphi} \tag{A.2}$$

into (3.7) and solving the remaining integral:

$$F_\varphi(\boldsymbol{r}, \varphi, t) = \frac{1}{(2\pi)^3} \sum_{p=-\infty}^{\infty} \int \mathrm{d}^2 k\, \hat{g}_p(\boldsymbol{k}, t) e^{-i\boldsymbol{k}\boldsymbol{r}} \int_\varphi^{\varphi+2\pi} \mathrm{d}\varphi_j e^{-ip\varphi_j} \left\{ 2s_0 \sin\left(\frac{\varphi - \varphi_j}{2}\right) \right.$$

$$\int_{l_c}^{l_s} \mathrm{d}r_{ji}\, r_{ji} \left[ \mu_m(r_{ji}) \int_{\frac{\varphi+\varphi_j}{2}}^{\frac{\varphi+\varphi_j}{2}+\pi} \mathrm{d}\alpha\, e^{-i\boldsymbol{k}\boldsymbol{r}_{ji}} \sin(\alpha - \varphi) \sin\left(\frac{\varphi + \varphi_j}{2} - \alpha\right) \right.$$

$$\left. -\mu_a(r_{ji}) \int_{\frac{\varphi+\varphi_j}{2}+\pi}^{\frac{\varphi+\varphi_j}{2}+2\pi} \mathrm{d}\alpha\, e^{-i\boldsymbol{k}\boldsymbol{r}_{ji}} \sin(\alpha - \varphi) \sin\left(\frac{\varphi + \varphi_j}{2} - \alpha\right) \right]$$

$$\left. - \int_0^{l_c} \mathrm{d}r_{ji}\, r_{ji}\, \mu_r(r_{ji}) \int_0^{2\pi} \mathrm{d}\alpha\, \sin(\alpha - \varphi) e^{-i\boldsymbol{k}\boldsymbol{r}_{ji}} \right\}. \tag{A.3}$$

In order to perform the integration, the exponential function $e^{-i\boldsymbol{k}\boldsymbol{r}_{ji}}$ is expanded into its Taylor series

$$e^{-i\boldsymbol{k}\boldsymbol{r}_{ji}} = \sum_{s=0}^{\infty} \frac{(-i)^s}{s!} (kr_{ji})^s \cos^s(\chi - \alpha), \tag{A.4}$$

where $\boldsymbol{k} = k\,(\cos\chi, \sin\chi)$ and $\boldsymbol{r}_{ji} = r_{ji}\,(\cos\alpha, \sin\alpha)$. Due to the isotropy of the uniform distribution (3.9), which stability is under consideration, $\chi = 0$ is chosen without loss of generality. Furthermore, it is convinient to use the following identity for $s \in \mathbb{N}$ [30]:

$$\cos^s(\alpha) = \frac{1}{2^s} \sum_{l=0}^{s} \binom{s}{l} \cos((s-2l)\alpha)\,. \tag{A.5}$$

Performing the integral yields the force expanded into a Fourier series and as a linear combination (A.1$b$) of the Fourier coefficients $\hat{g}_r(\boldsymbol{k}, t)$, where one can read off the elements of the infinite dimensional matrix $\tilde{K}_{p,n}(\boldsymbol{k})$:

$$
\begin{aligned}
\tilde{K}_{p,n}(\boldsymbol{k}) = {} & \frac{s_0\pi^2}{2i} \left[ (\mu_{m,0}(k) - \mu_{a,0}(k))\,(\delta_{p,1}\delta_{n,1} - \delta_{p,-1}\delta_{n,-1}) \right. \\
& + (\mu_{m,2}(k) - \mu_{a,2}(k))\,(\delta_{p,-1}\delta_{n,1} - \delta_{p,1}\delta_{n,-1} + (\delta_{p,2} - \delta_{p,-2})\,\delta_{n,0}) \big] \\
& - s_0 \sum_{s=0}^{\infty} \sum_{l=0}^{m} \left( \tilde{\mu}_m^{(2s+1)}(k) + \tilde{\mu}_a^{(2s+1)}(k) \right) \left[ \Lambda_{sl}^n\, \delta_{p+2l+1,n} - \Gamma_{sl}^n\, \delta_{p-2l-1,n} \right] \\
& + 2\pi^2 \tilde{\mu}_r(k)\delta_{n,0}\,(\delta_{p,1} - \delta_{p,-1})\,.
\end{aligned}
\tag{A.6}
$$

The following constants were introduced:

$$\mu_{m,\nu}(k) \quad = \int_{l_c}^{l_s} \mathrm{d}r_{ji}\, r_{ji}\, \mu_m(r_{ji}) J_\nu(k\,r_{ji})\,, \tag{A.7a}$$

$$\mu_{a,\nu}(k) \quad = \int_{l_c}^{l_s} \mathrm{d}r_{ji}\, r_{ji}\, \mu_a(r_{ji}) J_\nu(k\,r_{ji})\,, \tag{A.7b}$$

$$\tilde{\mu}_r(k) \quad = \int_0^{l_c} \mathrm{d}r_{ji}\, r_{ji}\, \mu_r(r_{ji}) J_1(k\,r_{ji})\,, \tag{A.7c}$$

$$\tilde{\mu}_{m,a}^{(2s+1)}(k) = \int_{l_c}^{l_s} \mathrm{d}r_{ji}\, r_{ji}\, \mu_{m,a}(r_{ji})(k\,r_{ji})^{2s+1}\,, \tag{A.7d}$$

$$\Lambda_{sl}^n \quad = \frac{(-1)^s}{2^{2s}} \frac{1}{(s-l)!(s+l+1)!} \left[ \frac{\alpha_{n-l}}{(2l-1)(2l+1)} - \frac{\alpha_{n-l-1}}{(2l+3)(2l+1)} \right]\,, \tag{A.7e}$$

$$\Gamma_{sl}^n \quad = \frac{(-1)^s}{2^{2s}} \frac{1}{(s-l)!(s+l+1)!} \left[ \frac{\alpha_{n+l}}{(2l-1)(2l+1)} - \frac{\alpha_{n+l+1}}{(2l+3)(2l+1)} \right]\,, \tag{A.7f}$$

$$\alpha_n \quad = \int_0^{2\pi} \mathrm{d}\xi\, \sin\left(\frac{\xi}{2}\right) e^{-in\xi} = \frac{4}{1-4n^2} \qquad (n \in \mathbb{Z})\,. \tag{A.7g}$$

The Bessel functions of the first kind are denoted by $J_\nu(x)$. Please note, that (A.6) is only valid for $\boldsymbol{k} = (k, 0)$.

## Appendix B. Transport Coefficients of (4.11)

The transport coefficients occuring in the hydrodynamic theory (4.11) are listed below.

$$\lambda_1 = \xi_1\rho - \xi_5 \tag{B.1a}$$

$$\lambda_2 = \frac{s_0}{2} \left( \frac{32}{9}\xi_3\rho - \xi_2\rho - s_0 \right) \tag{B.1b}$$

$$\lambda_3 = \frac{s_0}{8}\left(\xi_7 - \xi_6 + \frac{s_0 - \frac{32}{45}\xi_3\rho}{2\xi_5}\xi_4\rho\right) \tag{B.1c}$$

$$\lambda_4 = \frac{1}{4}\left[\frac{s_0 - \frac{32}{45}\xi_3\rho}{2\xi_5}\left(\frac{s_0}{2} + \frac{64}{45}\xi_3\rho\right) + \xi_4\rho\right] \tag{B.1d}$$

$$\lambda_5 = \frac{\xi_4\rho}{2} \tag{B.1e}$$

$$\eta_1 = \frac{\xi_1^2}{2\xi_5 s_0^2} \tag{B.1f}$$

$$\eta_2 = \frac{\xi_1}{4s_0\xi_5}\left(\frac{s_0}{2} + \frac{64}{45}\xi_3\rho\right) - \frac{32}{45s_0}\xi_3 + \frac{\frac{32}{45}\xi_3\rho - s_0}{2s_0\xi_5} \tag{B.1g}$$

$$\eta_3 = \frac{\xi_1}{4s_0\xi_5}\left(\frac{s_0}{2} + \frac{64}{45}\xi_3\rho\right) - \frac{32}{45s_0}\xi_3 - \frac{\frac{32}{45}\xi_3\rho - s_0}{2s_0\xi_5} \tag{B.1h}$$

$$\eta_4 = \frac{\xi_4}{2}\left(\frac{\xi_1\rho}{2\xi_5} - 1\right) \tag{B.1i}$$

$$\eta_5 = \frac{\frac{32}{45}\xi_3\rho - s_0}{8\xi_5}\left(\frac{32}{9}\xi_3 - \xi_2\right) - \frac{\xi_4}{4}\left(\frac{\xi_1\rho}{2\xi_5} - 1\right) \tag{B.1j}$$

$$\eta_6 = \frac{\xi_2 - \frac{32}{9}\xi_3}{2s_0\xi_5}\xi_1 \tag{B.1k}$$

$$\gamma_1 = -\frac{\left(\xi_2 - \frac{32}{9}\xi_3\right)^2}{8\xi_5} \tag{B.1l}$$

$$\gamma_2 = \frac{1}{4}\left(\frac{\xi_2 - \frac{32}{9}\xi_3}{2\xi_5}\left(\frac{s_0}{2} + \frac{64}{45}\xi_3\rho\right) + \frac{\frac{32}{45}\xi_3\rho - s_0}{2\xi_5}\frac{64}{45}\xi_3\right) + \frac{\frac{32}{45}\xi_3\rho - s_0}{8\xi_5}\left(\frac{32}{9}\xi_3 - \xi_2\right) \tag{B.1m}$$

$$\gamma_3 = -\frac{\frac{32}{45}\xi_3\rho - s_0}{4\xi_5}\left(\frac{32}{9}\xi_3 - \xi_2\right) \tag{B.1n}$$

$$\gamma_4 = -\frac{1}{4\xi_5}\left[\left(\xi_2 - \frac{32}{9}\xi_3\right)\left(\frac{s_0}{2} + \frac{64}{45}\xi_3\rho\right) + \left(\frac{32}{45}\xi_3\rho - s_0\right)\frac{64}{45}\xi_3\right] \tag{B.1o}$$

$$\gamma_5 = \frac{s_0\xi_4 - \xi_2\xi_4\rho + \frac{128}{45}\xi_3\xi_4\rho}{16\xi_5} \tag{B.1p}$$

## References

[1] V. Schaller, C. Weber, C. Semmrich, E. Frey, and A. R. Bausch. Polar patterns of driven filaments. *Nature*, 467(7311):73–77, 2010.

[2] G. Salbreux, G. Charras, and E. Paluch. Actin cortex mechanics and cellular morphogenesis. *Trends in Cell Biology*, 22(10):536–545, October 2012.

[3] H. H. Wensink, J. Dunkel, S. Heidenreich, K. Drescher, R. E. Goldstein, H. Löwen, and J. M. Yeomans. Meso-scale turbulence in living fluids. *Proceedings of the National Academy of Sciences*, 109(36):14308–14313, September 2012.

[4] F. Peruani, J. Starruß, V. Jakovljevic, L. Søgaard-Andersen, A. Deutsch, and M. Bär. Collective motion and nonequilibrium cluster formation in colonies of gliding bacteria. *Physical Review Letters*, 108(9):098102, February 2012.

[5] I. Theurkauff, C. Cottin-Bizonne, J. Palacci, C. Ybert, and L. Bocquet. Dynamic clustering in active colloidal suspensions with chemical signaling. *Physical Review Letters*, 108(26):268303, June 2012.

[6] A. Kudrolli, G. Lumay, D. Volfson, and L. S. Tsimring. Swarming and swirling in self-propelled polar granular rods. *Physical Review Letters*, 100(5):058001, February 2008.

[7] J. Deseigne, O. Dauchot, and H. Chaté. Collective motion of vibrated polar disks. *Physical Review Letters*, 105(9):098001, 2010.

[8] M. Ballerini, N. Cabibbo, R. Candelier, A. Cavagna, E. Cisbani, I. Giardina, V. Lecomte, A. Orlandi, G. Parisi, A. Procaccini, M. Viale, and V. Zdravkovic. Interaction ruling animal collective behavior depends on topological rather than metric distance: Evidence from a field study. *Proceedings of the National Academy of Sciences*, 105(4):1232 –1237, January 2008.

[9] U. Lopez, J. Gautrais, I. D. Couzin, and G. Theraulaz. From behavioural analyses to models of collective motion in fish schools. *Interface Focus*, October 2012.

[10] J. Buhl, D. J. T. Sumpter, I. D. Couzin, J. J. Hale, E. Despland, E. R. Miller, and S. J. Simpson. From disorder to order in marching locusts. *Science*, 312(5778):1402–1406, June 2006.

[11] S. Bazazi, P. Romanczuk, S. Thomas, L. Schimansky-Geier, J. J. Hale, G. A. Miller, G. A. Sword, S. J. Simpson, and I. D. Couzin. Nutritional state and collective motion: from individuals to mass migration. *Proceedings of the Royal Society B: Biological Sciences*, 278(1704):356 –363, February 2011.

[12] T. Vicsek, A. Czirók, E. Ben-Jacob, I. Cohen, and O. Shochet. Novel type of phase transisition in a system of Self-Driven particles. *Physical Review Letters*, 75(6):1226–1229, 1995.

[13] J. Toner and Y. Tu. Long-Range order in a two-dimensional dynamical XY model: How birds fly together. *Physical Review Letters*, 75(23):4326, 1995.

[14] J. Toner and Y. Tu. Flocks, herds, and schools: A quantitative theory of flocking. *Physical Review E*, 58(4):4828–4858, 1998.

[15] J. Toner, Y. Tu, and S. Ramaswamy. Hydrodynamics and phases of flocks. *Annals of Physics*, 318(1):170–244, July 2005.

[16] S. Ramaswamy. The mechanics and statistics of active matter. *Annual Review of Condensed Matter Physics*, 1(1):323–345, August 2010.

[17] E. Bertin, M. Droz, and G. Grégoire. Boltzmann and hydrodynamic description for self-propelled particles. *Physical Review E (Statistical, Nonlinear, and Soft Matter Physics)*, 74(2):022101–4, 2006.

[18] E. Bertin, M. Droz, and G. Grégoire. Microscopic derivation of hydrodynamic equations for self-propelled particles. *Journal of Physics A: Mathematical and Theoretical*, 42:445001, 2009.

[19] T. Ihle. Kinetic theory of flocking: Derivation of hydrodynamic equations. *Physical Review E*, 83(3):030901, March 2011.

[20] A. Peshkov, S. Ngo, E. Bertin, H. Chaté, and F. Ginelli. Continuous theory of active matter systems with metric-free interactions. *Phys. Rev. Lett.*, 109:098101, August 2012.

[21] A. Peshkov, I. S. Aranson, E. Bertin, H. Chaté, and F. Ginelli. Nonlinear field equations for aligning self-propelled rods. *Physical Review Letters*, 109(26):268701, December 2012.

[22] F. D. C. Farrell, M. C. Marchetti, D. Marenduzzo, and J. Tailleur. Pattern formation in self-propelled particles with density-dependent motility. *Phys. Rev. Lett.*, 108:248101, June 2012.

[23] R. Großmann, L. Schimansky-Geier, and P. Romanczuk. Active brownian particles with velocity-alignment and active fluctuations. *New Journal of Physics*, 14(7):073033, 2012.

[24] P. Romanczuk and U. Erdmann. Collective motion of active brownian particles in one dimension. *The European Physical Journal Special Topics*, 187(1):127–134, October 2010.

[25] P. Romanczuk and L. Schimansky-Geier. Mean-field theory of collective motion due to velocity alignment. *Ecological Complexity*, 10:83–92, June 2012.

[26] S. Mishra, K. Tunstrøm, I. D. Couzin, and C. Huepe. Collective dynamics of self-propelled particles with variable speed. *Phys. Rev. E*, 86:011901, July 2012.

[27] V. Guttal, P. Romanczuk, S. J. Simpson, G. A. Sword, and I. D. Couzin. Cannibalism can drive the evolution of behavioural phase polyphenism in locusts. *Ecology Letters*, 15(10):1158–1166, 2012.

[28] P. Romanczuk and L. Schimansky-Geier. Swarming and pattern formation due to selective

attraction and repulsion. *Interface Focus*, 2(6):746–756, September 2012.

[29] Y.-L. Chou, R. Wolfe, and T. Ihle. Kinetic theory for systems of self-propelled particles with metric-free interactions. *Phys. Rev. E*, 86:021120, August 2012.

[30] I. N. Bronstein, K.A. Semendjajew, M. Gerhard, and H. Mühlig. *Taschenbuch der Mathematik*. Verlag Harri Deutsch, Frankfurt am Main, 7 edition, 2008.

[31] I. S. Aranson and L. S. Tsimring. Pattern formation of microtubules and motors: Inelastic interaction of polar rods. *Phys. Rev. E*, 71:050901, May 2005.

[32] S. Sankararaman, G. I. Menon, and P. B. Sunil Kumar. Self-organized pattern formation in motor-microtubule mixtures. *Phys. Rev. E*, 70:031905, September 2004.

[33] P. Romanczuk, I. D. Couzin, and L. Schimansky-Geier. Collective motion due to individual escape and pursuit response. *Physical Review Letters*, 102(1):010602–4, January 2009.

[34] S. Ramaswamy, R. A. Simha, and J. Toner. Active nematics on a substrate: Giant number fluctuations and long-time tails. *Europhysics Letters (EPL)*, 62(2):196–202, April 2003.

[35] A. Baskaran and M. C. Marchetti. Hydrodynamics of self-propelled hard rods. *Physical Review E*, 77(1):011920, January 2008.

[36] F. Ginelli, F. Peruani, M. Bär, and H. Chaté. Large-scale collective properties of self-propelled rods. *Physical Review Letters*, 104(18):184502, 2010.

[37] S. Mishra, R. A. Simha, and S. Ramaswamy. A dynamic renormalization group study of active nematics. *Journal of Statistical Mechanics: Theory and Experiment*, 2010(02):P02003, February 2010.

[38] A. Mikhailov and D. Meinköhn. Self-motion in physico-chemical systems far from thermal equilibrium. In Lutz Schimansky-Geier and Thorsten Pöschel, editors, *Stochastic Dynamics*, volume 484 of *Lecture Notes in Physics*, pages 334–345. Springer Berlin Heidelberg, 1997.

[39] P. Romanczuk, M. Bär, W. Ebeling, B. Lindner, and L. Schimansky-Geier. Active brownian particles. *The European Physical Journal Special Topics*, 202(1):1–162, March 2012.